NANO LETTERS

2007
Vol. 7, No. 4
1013−1017

The SERS Activity of a Supported Ag Nanocube Strongly Depends on Its Orientation Relative to Laser Polarization

Joseph M. McLellan, Zhi-Yuan Li,† Andrew R. Siekkinen, and Younan Xia*

Department of Chemistry, University of Washington, Seattle, Washington 98195-1700

Received January 19, 2007; Revised Manuscript Received March 12, 2007

ABSTRACT

Silver nanocubes with sharp or truncated corners were synthesized, deposited on silicon substrates, and functionalized with Raman-active thiols for surface-enhanced Raman scattering (SERS) studies. The use of substrates with registration marks allowed us to correlate the SERS spectra from individual nanocubes to their physical parameters revealed by high-resolution SEM imaging. We observed dramatic variations in SERS intensity when the nanocubes were oriented at different angles relative to the polarization of excitation laser. This angular dependence was less significant when the nanocubes were truncated and became nearly spherical in profile. Numerical calculations were employed to confirm our observations, and to attribute the source of variation to the difference in near-field distribution between different laser polarizations.

The role of localized surface plasmon resonance (LSPR) in surface-enhanced Raman scattering (SERS) has been clearly established for many years.[1−4] It is generally accepted that the local field that develops on the surface of a metal nanoparticle when it interacts with the incident light is primarily responsible for the SERS effect. The enhancement will be maximized when the wavelength of incident light is in resonance with the LSPR band of the nanoparticle.[5,6] The LSPR properties of a metal nanoparticle is strongly dependent on several factors including the size, shape, dielectric environment, and proximity to other particles as well as orientation relative to the polarization of incident light.[7−15] Any polydispersity in size and shape of the particles may lead to variations in the overall SERS activity of the ensemble. The random formation of "hot spots" through plasmonic coupling of closely spaced particles is expected to be the most significant source of variation.[14−19] The local fields in such hot spots can be orders of magnitude stronger than those on individual particles and have enabled the giant enhancement required for single molecule detection.[16,17] While calculations have confirmed that the field enhancement in a hot spot can account for the observation of single molecules by SERS,[20] Nie and Emory found that a small portion of single silver particles could also be extremely Raman active with an enhancement factor high enough for single molecule detection.[21] However, the origin of this extraordinary enhancement is yet to be uncovered. A systematic study on the relationship between the Raman scattering intensity and the physical parameters of a nanoparticle could eventually lead to an understanding of why certain particles are hot while others are not. In this regard, experiments capable of correlating the optical response with high-resolution imaging should be helpful in attaining a better understanding of the complex physics behind the enhancement process.

It is worth noting that theoretical calculations of optical properties of metal nanoparticles with arbitrary shapes have already reached a fairly high level of maturity.[20,22] These calculations are typically conducted for single particles with well-defined compositions, sizes, shapes, and spatial orientations relative to the polarization of incident light. As a result, SERS experiments on single nanoparticles could provide a direct comparison between experimental and theoretical results. Here we report SERS measurements on individual Ag nanocubes with different orientations relative to the polarization of excitation laser. While significant variations were found for the SERS activities of individual nanocubes with sharp corners, the intensity of SERS signals from rounded particles showed little difference. Additionally, we have conducted calculations for both the far-field extinction spectra and near-field distributions to further confirm these results.

Several approaches have been demonstrated to correlate both elastic and inelastic scattering measurements to the morphology of a nanoparticle. These include the use of

* Corresponding author. E-mail: xia@chem.washington.edu.
† Institute of Physics, Chinese Academy of Sciences, Beijing 100080, P. R. China.

10.1021/nl070157q CCC: $37.00
Published on Web 03/22/2007

instruments that allow for simultaneous optical and atomic force microscopy (AFM) characterization[21,23−25] as well as the use of registration marks on a substrate[26−29] or pattern recognition[30,31] to help correlate the optical and structural measurements. While the use of an instrument that allows for in situ optical and AFM experiments is elegant, AFM imaging alone cannot easily resolve the exact profile of a nanoparticle due to tip convolution. In comparison, electron microscopy (both scanning and transmission) provides a definite advantage. For this reason, several groups have employed registration marks on substrates for ex situ correlation of optical with electron microscopy measurements. These experiments have primarily utilized the high-resolution power of transmission electron microscopy (TEM) for structural characterization. It appears to us that scanning electron microscopy (SEM) might be more convenient for the correlated measurements because it can be easily operated to obtain similar details about the morphology of a nanoparticle (see Figure S1, Supporting Information, for a comparison between SEM and TEM images of Ag nanocubes). More importantly, one can use conductive Si substrates patterned with a simple array of microscale registration marks as the supports for correlated SERS/SEM measurements. The registration marks can be readily fabricated using photolithography, followed by thermal evaporation of a metal (e.g., Au or Al) and lift-off. The result is a substrate that is inexpensive, simple to fabricate, structurally robust, and easily handled (compared to TEM grids). The marks allow one to readily locate the same nanoparticle when going between Raman and electron microscopes. In general, this approach allows for the use of SEM, AFM, or both to further characterize the region of interest following Raman characterization, albeit we only focus on SEM in this work.

The first step involved synthesis of Ag nanocubes with sharp or truncated corners using our previously published procedures (see the Supporting Information for experimental details).[32,33] Briefly, $AgNO_3$ was reduced by ethylene glycol (EG) at 150 °C in the presence of poly(vinyl pyrrolidone) (PVP) and HCl. The EG served as both reductant and solvent, while HCl mainly acted as an oxidative etchant. The mixture was allowed to react for 24 h, and the products, Ag nanocubes with sharp corners, were collected by centrifugation. The nanocubes were washed with acetone and ethanol to remove EG and excess PVP, and then redispersed in water for further use. The truncated versions of these sharp cubes were obtained by dispersing them in a 1 mM solution of HCl in EG and heating to 145 °C for 5 min. A small amount of PVP (0.1 mM) was also added to help stabilize the suspension. The truncated nanocubes were finally washed with acetone and ethanol, centrifuged, and redispersed in water. Samples for correlated SEM and SERS experiments were prepared by drop-casting a dilute aqueous suspension of the Ag nanocubes on Si substrates that had been patterned with registration marks and letting them dry under ambient conditions. Once the samples had dried, they were immersed in a 1 mM solution of 1,4-benzenedithiol (1,4-BDT, Aldrich) in ethanol for 1 h, taken out, washed with copious amounts of ethanol, and finally dried with a stream of air. All samples were used within 24 h after preparation.

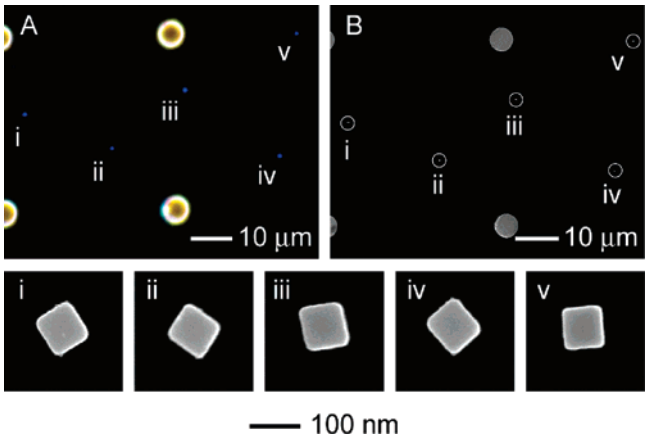

Figure 1. (A) Dark-field optical micrograph of a substrate with registration marks (large yellow spots) and a number of individual Ag nanocubes (small blue dots) labeled i−v. (B) SEM image of the same region as shown in (A). Below (A) and (B) are SEM images that clearly resolve the morphology of each individual Ag nanocube. Note that the 100 nm scale bar applies to all the high-magnification SEM images.

Figure 1 demonstrates how we correlated the SERS spectra from individual particles to their SEM images. Figure 1A shows a dark-field optical micrograph of a region containing a number of sharp Ag nanocubes (the blue dots labeled i−v) and several registration marks (the larger yellow spots). Figure 1B shows an SEM image of the same region shown in Figure 1A. The particles are also circled and labeled in the SEM image to help identify them. SEM images of these cubes at a higher magnification are shown in the strip of images below panels A and B.

Using this approach, we recorded SERS spectra and SEM images from many individual particles. Figure S2, Supporting Information, shows the correlated SERS spectra and SEM images from 10 typical nanocubes with random orientations relative to the polarization of the incident laser. All spectra in this study were obtained with a 514 nm argon laser (2 mW at the sample) using a dry 50× objective (NA = 0.80) in single static scans with an acquisition time of 30 s (see Supporting Information for more details). In the spectra, the broad band at 900−1000 cm^{-1} can be attributed to the Si substrate and was used in this work as a reference for intensity normalization. The peaks at other positions (1080, 1180, and 1565 cm^{-1}) can be ascribed to the vibrations of 1,4-BDT.[33−35] More specifically, the bands at 1565 and 1180 cm^{-1} were assigned to modes ν_{8a} and ν_{9a}, while the band at 1080 cm^{-1} can be ascribed to the ν_1 fundamental in Fermi resonance with a combination mode consisting of $\nu_{6a} + \nu_{7a}$.[33,34] For the 30 individual cubes investigated, we found an average edge length of 97.3 nm and a standard deviation of 5 nm. Despite the high-level of monodispersity for these cubes, the SERS signals could vary significantly from cube to cube. When we examine the spectra and take into consideration the orientation of the particles relative to the laser polarization during spectral acquisition, we noticed an interesting trend. It appears that the variation in SERS activity

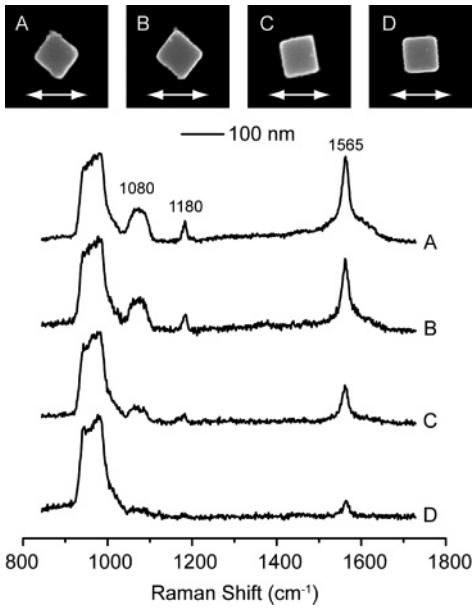

Figure 2. SEM images labeled (A−D) are of individual Ag nanocubes that had been deposited on a registered substrate and then functionalized with 1,4-BDT. The 100 nm scale bar applies to all images. The white arrows in the images denote the polarization direction of the incident laser. The corresponding SERS spectra from these particles are stacked below the SEM images.

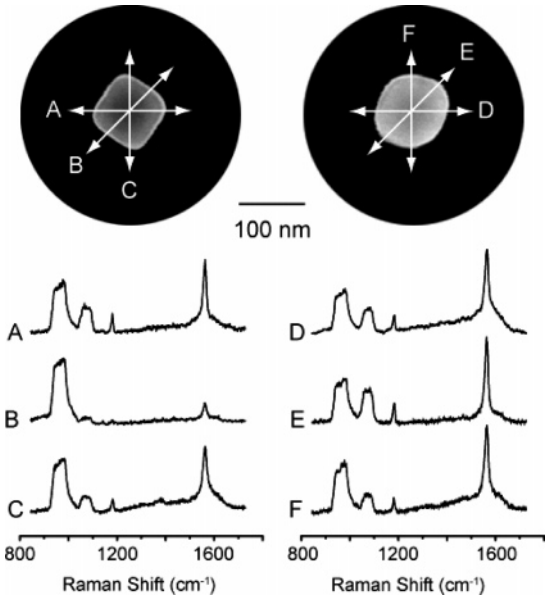

Figure 3. Normalized SERS spectra of 1,4-BDT adsorbed on a Ag nanocube with sharp corners (left panel, A−C) and a highly truncated Ag nanocube (right panel, D−F), at various angles relative to the polarization of the excitation laser. Each SEM image shows the nanocube used and the arrows indicate the polarization directions of incident laser corresponding to the spectra. The scale bar applies to both images. The spectra were stacked with off-set for clarity.

for these cubes mainly came from the difference in local field strength as the cube is randomly oriented relative to the polarization of excitation laser. For example, Figure 2 shows SEM images of four cubes and their corresponding SERS spectra. The white arrows in the SEM images denote the polarization of the incident laser. It is clear that individual nanocubes with sharp corners were most active when they were oriented such that a diagonal axis (corner to corner) of the cube (particles A and B in Figure 2) was parallel to the polarization of the laser. As shown by particles C and D in Figure 2, nanocubes that were oriented with one of their faces parallel to the laser polarization were much less active.

To further illustrate this effect, we measured the SERS spectra from 1,4-BDT adsorbed on a single Ag nanocube with sharp corners at different azimuthal angles relative to the polarization of excitation laser. Figure S3, Supporting Information, shows a photograph of a stage specially designed for such measurements. The results of these experiments are shown in Figure 3. When the sharp cube was orientated with a diagonal axis (corner to corner) parallel to the laser polarization (A and C), the signal was much higher than when the cube was oriented with one of the faces parallel to the polarization of the laser (B). We also conducted the same experiment on a highly truncated cube. It is clear that the SERS spectra for the truncated cube (D−F) was essentially unaffected, while the sharp cube (A−C) showed dramatic variations as their orientations were changed relative to the polarization of the laser. Because the cubes take random orientations when they were deposited on a substrate and the laser polarization is fixed, this is a significant source of intensity variation.

To understand the dependence of SERS signal on laser polarization, we conducted both far- and near-field calculations for a 100 nm Ag cube and sphere (suspended in air) that approximate the experimental conditions in Figure 3. For the Ag cube, the discrete-dipole approximation (DDA) method was used to calculate the far-field extinction spectra and the near-field distributions at an excitation wavelength of 514 nm. We used 64 000 dipoles to approximate the nanocube, with the incident light polarized along both [100] and [110] directions. For the Ag sphere, Mie theory was employed to calculate the extinction spectra as well as the near-field distribution when the sphere is irradiated at a wavelength of 514 nm. The results of these calculations are shown in Figure 4. Panel A shows the E-field amplitude pattern for a cube that is irradiated with light polarized in the [100] direction, and panel B shows the E-field pattern when the light is polarized in the [110] direction. These calculations clearly show that the near-field distribution for a cube has a strong dependence on polarization. As shown by the data in panel D, the far-field extinction spectra have no dependence on polarization for both the cube and the sphere.

For the cube, the $|E|_{max}$ at [100] polarization was 26.5, while the value was 37.8 for [110] polarization. This would indicate that the [110] polarization could generate a maximum SERS enhancement that was 4 times that of the [100] polarization, as SERS is proportional to $|E|^4$. However, because the field is not uniform, the field amplitude averaged over the particle's surface is perhaps a more useful value in predicting the SERS enhancement that is observed per particle. In this case, the average $|E|^4$ values for the [100] and [110] polarizations were 2653 and 5154, respectively. These results not only confirm the polarization dependence observed for the SERS signal but also suggest that the signal

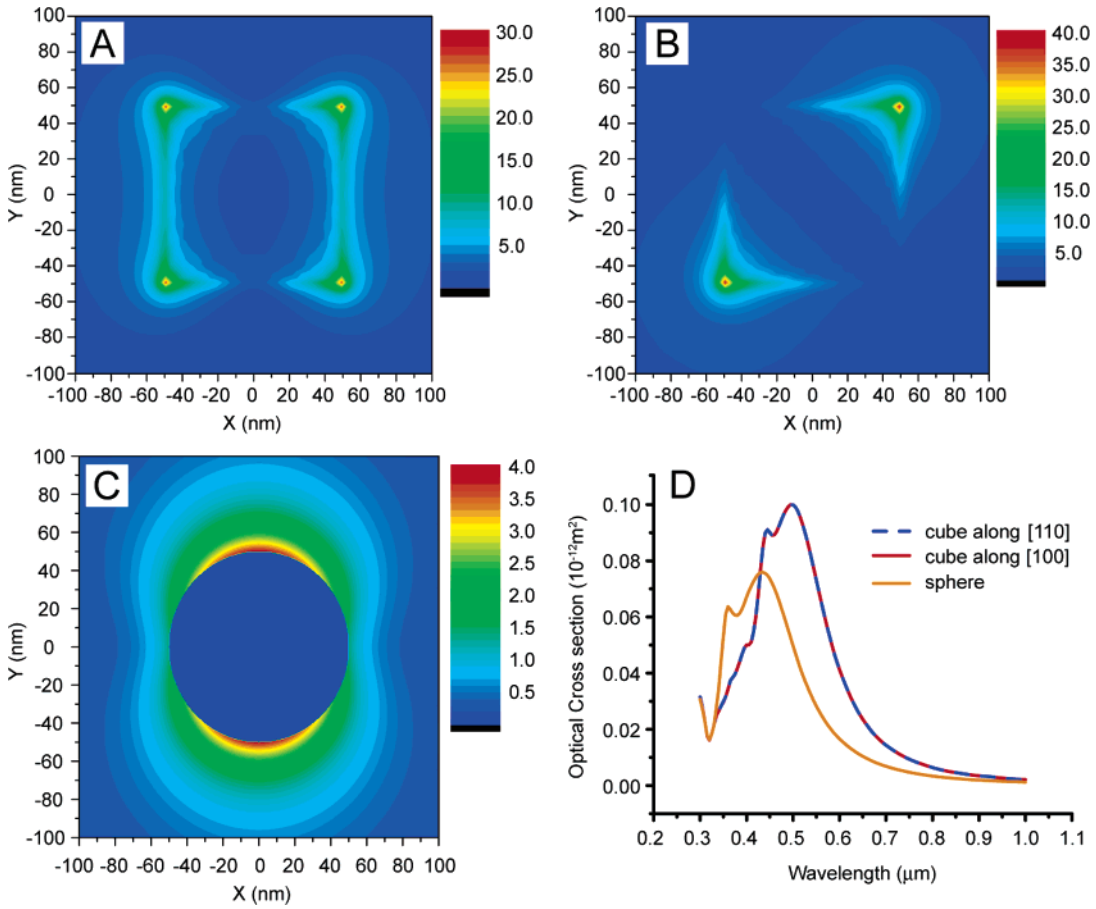

Figure 4. (A−C) E-field amplitude (|E|) patterns for a 100 nm Ag cube at two polarizations and a 100 nm Ag sphere when irradiated at a wavelength of 514 nm: (A) 100 nm Ag cube, with the incident light along the *z*-axis and the E-field along the *x*-axis or [100] direction; (B) 100 nm Ag cube, with the incident light along the *z*-axis and E-field along the [110] direction; and (C) 100 nm Ag sphere, with the incident light along the *z*-axis and E-field along the *x*-axis. The incident field amplitude was assumed to be 1. (D) Far-field extinction spectra calculated for a 100 nm Ag sphere in air (solid orange line) and a 100 nm Ag cube excited at two polarizations: [110] (blue dashed line) and [100] (solid red line). All spectra were calculated for particles suspended in air.

variation is mainly caused by difference in near-field distribution between different polarizations.

We have also examined how the shape of an individual particle affects the SERS intensity. Figure 5 compares the SERS spectra taken from four individual Ag nanoparticles of different geometries: a right bipyramid, a cube with sharp corners, and two truncated cubes. The right bipyramids are a common side-product (up to ∼10%) in a typical synthesis of Ag nanocubes. We found it difficult to identify these particles by optical microscopy alone, yet ended up sampling several of them when targeting single cubes. A typical example is shown in panel A. It is clear that the cube with sharp corners and the right bipyramid produced similar Raman intensity, while truncated cubes gave much stronger Raman peaks under the same experimental conditions. The integrated area of the 1565 cm^{-1} band for the sharp cube is 3.56× less than that for the truncated cube shown in panel D. On the basis of the SEM images, particle C is significantly truncated as compared to particle B, and particle D is more truncated than particle C because the facets are no longer visible for particle D. In a recent study, we examined the SERS activities of both sharp and truncated Ag nanocubes

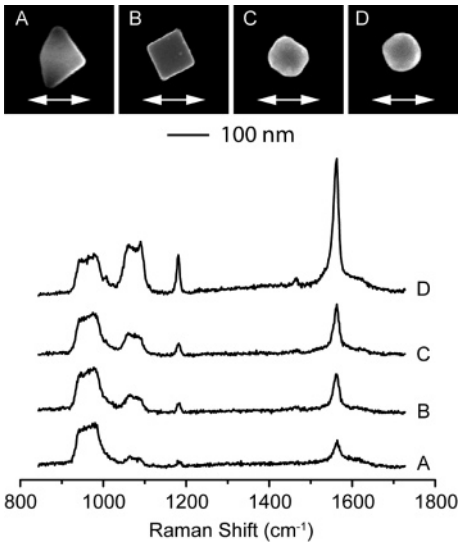

Figure 5. Comparison of SERS spectra of 1,4-BDT adsorbed on single Ag nanoparticles with different morphologies: (A) right bipyramid, (B) cube with sharp corners, and (C,D) truncated cubes, as shown in the accompanying SEM images. The spectra were stacked with offset for clarity.

in aqueous solutions and found surface-enhancement factors of 1.25×10^5 and 8.53×10^4 for 100 nm sharp and truncated nanocubes, respectively.[33] While it may not necessarily make sense to compare the spectra taken from single particles with fixed orientations and the directionally averaged solution-phase ensemble measurements, the solution-phase results were consistent with theoretical predictions. The observation of higher SERS activity for a supported truncated cube as compared to a supported cube with sharp corners is interesting because it is contrary to the theoretical prediction and to previous studies. We do not yet understand this trend, but are currently pursuing investigations in this direction.

In summary, we have utilized substrates with registration marks to correlate the SERS spectra from individual Ag nanocubes to their physical parameters revealed by high-resolution SEM imaging. While the nanocubes used in this study were monodispersed in size and shape, the SERS signals recorded from different nanocubes showed considerable variations in intensity. Backed up by calculations, we have shown that this variation can be attributed to the difference in near-field distribution when the nanocube takes different orientation relative to the laser polarization. We have also shown that the importance of this effect is highly dependent on the degree of truncation for the cubes, with the sharp ones being more sensitive to the orientation than their truncated, nearly spherical counterparts. This angular dependence of SERS activities for Ag nanocubes suggests that the laser polarization needs to be taken into account whenever supported, nonspherical nanoparticles are involved.

Acknowledgment. This work was initiated through a student fellowship from the NIH-funded MLSC program at the UW. It was supported in part by a fellowship from the David and Lucile Packard Foundation and GEMSEC (Genetically Engineered Materials Science and Engineering Center), an NSF-supported MRSEC program at the UW. Y.X. is a Camille Dreyfus Teacher Scholar (2002-2007). Instrumentation was provided by the Nanotech User Facility (NTUF), a member of the National Nanotechnology Infrastructure Network (NNIN) supported by the NSF. We also thank the NTUF staff for technical support. Z.Y.L. thanks the National Natural Science Foundation of China (no. 10525419) for financial support.

Supporting Information Available: Experimental details; figures showing a comparison of TEM and SEM images, SERS spectra from 10 individual Ag nanocubes, and a digital photograph of the rotational stage. This material is available free of charge via the Internet at http://pubs.acs.org.

References

(1) Haynes, C. L.; Van Duyne, R. P. *J. Phys. Chem. B* **2003**, *107*, 7426.
(2) Jackson, J. B.; Halas, N. J. *Proc. Natl. Acad. Sci. U.S.A.* **2004**, *101*, 17930.
(3) Haes, A. J.; Haynes, C. L.; McFarland, A. D.; Schatz, G. C.; Van Duyne, R. P.; Zou, S. *MRS Bull.* **2005**, *30*, 368.
(4) McLellan, J. M.; Xiong, Y.; Hu, M.; Xia, Y. *Chem. Phys. Lett.* **2006**, *417*, 230.
(5) Schwartzberg, A. M.; Grant, C. D.; Wolcott, A.; Talley, C. E.; Huser, T. R.; Bogomolni, R.; Zhang, J. Z. *J. Phys. Chem. B* **2004**, *108*, 19191.
(6) Halas, N. J. *MRS Bull.* **2005**, *30*, 362.
(7) (a) Sun, Y.; Xia, Y. *J. Am. Chem. Soc.* **2004**, *126*, 3892. (b) Wiley, B. J.; Im, S. H.; Li, Z. Y.; McLellan, J. M.; Siekkinen, A.; Xia, Y. *J. Phys. Chem. B* **2006**, *110*, 15666.
(8) Sun, Y.; Xia, Y. *Analyst* **2003**, *128*, 686.
(9) (a) Wiley, B.; Im, S. H.; Li, Z. Y.; McLellan, J. M.; Siekkinen, A.; Xia, Y. *J. Phys. Chem. B* **2006**, *110*, 15666. (b) Wiley, B.; Sun, Y.; Mayers, B.; Xia, Y. *Chem.—Eur. J.* **2005**, *11*, 454.
(10) (a) Xiong, Y.; Wiley, B.; Chen, J.; Li, Z. Y.; Yin, Y.; Xia, Y. *Angew. Chem., Int. Ed.* **2005**, *44*, 7913. (b) McLellan, J. M.; Xiong, Y.; Hu, M.; Xia, Y. *Chem. Phys. Lett.* **2006**, *417*, 230. (c) Xiong, Y.; McLellan, J. M.; Chen, J.; Yin, Y.; Li, Z. Y.; Xia, Y. *J. Am. Chem. Soc.* **2005**, *127*, 17118.
(11) Jensen, T. R.; Malinsky, M. D.; Haynes, C. L.; Van Duyne, R. P. *J. Phys. Chem. B* **2000**, *104*, 10549.
(12) Oldenburg, S. J.; Jackson, J. B.; Westscott, S. L.; Halas, N. J. *Science* **2003**, *302*, 419.
(13) Chen, J.; Wiley, B.; McLellan, J. M.; Xiong, Y.; Li, Z. Y.; Xia, Y. *Nano Lett.* **2005**, *5*, 2058.
(14) Kneipp, K.; Kneipp, H.; Manoharan, R.; Hanlon, E. B.; Itzkan, I.; Dasari, R. R.; Feld, M. S. *Appl. Spectrosc.* **1998**, *52*, 1493.
(15) (a) Xu, H. X.; Käll, M. *ChemPhysChem* **2003**, *4*, 1001. (b) Xu, H. X.; Azpurua, J.; Käll, M. J.; Apell, P. *Phys. Rev. E* **2000**, *62*, 4318.
(16) Wang, Z.; Pan, S.; Krauss, T. D.; Du, H.; Rothberg, L. J. *Proc. Natl. Acad. Sci. U.S.A.* **2003**, *100*, 8638.
(17) Kneipp, K.; Wang, Y.; Dasari, R. R.; Feld, M. S. *Appl. Spectrosc.* **1995**, *49*, 780.
(18) (a) Kuncicky, D. M.; Christesen, S. D.; Velev, O. D. *Appl. Spectrosc.* **2005**, *59*, 401. (b) Tessier, P. M.; Velev, O. D.; Kalambur, A. T.; Rabolt, J. F.; Lenhoff, A. M.; Kaler, E. W. *J. Am. Chem. Soc.* **2000**, *122*, 9554.
(19) Tao, A.; Kim, F.; Hess, C.; Goldberger, J.; He, R.; Sun, Y.; Xia, Y.; Yang, P. *Nano Lett.* **2003**, *3*, 1229.
(20) (a) Zou, S.; Schatz, G. C. *Chem. Phys. Lett.* **2005**, *403*, 62. (b) Schatz, G. C.; Young, M. A.; Van Duyne, R. P. In *Surface Enhanced Raman Scattering Physics and Applications;* Kneipp, K., Moskovits M., Kneipp, H., Eds.; Topics in Applied Physics; Springer: New York, 2006; Vol. 103, pp 19−46.
(21) Nie, S. M.; Emory, S. R. *Science* **1997**, *275*, 1102.
(22) (a) Kelly, K. L.; Coronado, E.; Zhao, L. L.; Schatz, G. C. *J. Phys. Chem. B* **2003**, *107*, 668. (b) Sherry, L. J.; Chang, S. H.; Schatz, G. C.; Van Duyne, R. P.; Wiley, B. J.; Xia, Y. *Nano Lett.* **2005**, *5*, 2034.
(23) Michaels, A. M.; Jiang, J.; Brus, L. *J. Am. Chem. Soc.* **2000**, *104*, 11965.
(24) (a) Lu, H. P. *J. Phys.: Condens. Matter* **2005**, *17*, R333. (b) Hu, D.; Micic, M.; Klymyshyn, N.; Suh, Y. D.; Lu, H. P. *Rev. Sci. Instrum.* **2003**, *74*, 3347.
(25) Talley, C. E.; Jackson, J. B.; Oubre, C.; Grady, N. K.; Hollars, C. W.; Lane, S. M.; Huser, T. R.; Nordlander, P.; Halas, N. J. *Nano Lett.* **2005**, *5*, 1569.
(26) (a) Khan, I.; Cunningham, D.; Graham, D.; McComb, D. W.; Smith, W. E. *J. Phys. Chem. B* **2005**, *109*, 3454. (b) Khan, I.; Polwart, E.; McComb, D. W.; Smith, W. E. *Analyst* **2004**, *129*, 950.
(27) Nehl, C. L.; Grady, N. K.; Goodrich, G. P.; Tam, F.; Halas, N. J.; Hafner, J. H. *Nano Lett.* **2004**; *4*, 2355.
(28) Maruyama, Y.; Futamata, M. *J. Raman Spectrosc.* **2005**, *36*, 581.
(29) Jin, R.; Jureller, J. E.; Scherer, N. F. *Appl. Phys. Lett.* **2006**, *88*, 263111.
(30) Mock, J. J.; Barbic, M.; Smith, D. R.; Schultz, D. A.; Schultz, S. *J. Chem. Phys.* **2002**, *116*, 6755.
(31) Khan, I.; Cunningham, D.; Littleford, R. E.; Graham, D.; Smith, W. E.; McComb, D. W. *Anal. Chem.* **2006**, *78*, 224.
(32) (a) Im, S. H.; Lee, Y. T.; Wiley, B.; Xia, Y. *Angew. Chem., Int. Ed.* **2005**, *44*, 2154. (b) Sun, Y.; Xia, Y. *Science* **2002**, *298*, 2176.
(33) McLellan, J. M.; Siekkinen, A.; Chen, J.; Xia, Y. *Chem. Phys. Lett.* **2006**, *427*, 122.
(34) (a) Joo, S. W.; Han, S. W.; Kim, K. *J. Colloid Interface Sci.* **2001**, *240*, 391. (b) Cho, S. H.; Han, H. S.; Jang, D. J.; Kim, K.; Kim, M. S. *J. Phys. Chem.* **1995**, *99*, 10594.
(35) Moskovits, M.; Jeong, D. H. *Chem. Phys. Lett.* **2004**, *397*, 91.

NL070157Q